Aerospace Science and Technology 16 (2012) 29–39

Contents lists available at ScienceDirect

Aerospace Science and Technology

www.elsevier.com/locate/aescte

Helicopter aeroelastic analysis with spatially uncertain rotor blade properties

Senthil Murugan *, R. Chowdhury, S. Adhikari, M.I. Friswell

School of Engineering, Swansea University, Singleton Park, Swansea SA2 8PP, UK

ARTICLE INFO

Article history:
Received 30 September 2010
Received in revised form 20 December 2010
Accepted 10 February 2011
Available online 18 February 2011

Keywords:
Uncertainty analysis
Composites
Helicopter aeroelasticity
High-dimensional model representation

ABSTRACT

This paper investigates the effects of spatially uncertain material properties on the aeroelastic response predictions (e.g., rotating frequencies, vibratory loads, etc.) of composite helicopter rotor. Initially, the spatial uncertainty is modeled as discrete random variables along the blade span and uncertainty analysis is performed with direct Monte Carlo simulations (MCS). Uncertainty effects on the rotating frequencies vary with the higher-order modes in a non-linear way. Each modal frequency is found to be more sensitive to the uncertainty at certain sections of the rotor blade than uncertainty at other sections. Uncertainty effects on the vibratory hub load predictions are studied in the next stage. To reduce the computational expense of stochastic aeroelastic analysis, a high-dimensional model representation (HDMR) method is developed to approximate the aeroelastic response as functions of blade stiffness properties which are modeled as random fields. Karhunen–Loève expansion and a lower-order expansion are used to represent the input and outputs, respectively, in the HDMR formulation which is similar to the spectral stochastic finite element method. The proposed method involves the approximation of the system response with lower-dimensional HDMR, the response surface generation of HDMR component functions, and Monte Carlo simulation. The proposed approach decouples the computationally expensive aeroelastic simulations and uncertainty analysis. MCS, performed with computationally less expensive HDMR models, shows that spatial uncertainty has considerable influence on the vibratory hub load predictions.

1. Introduction

Composite materials are extensively used in the design of aircraft structures because of their high stiffness to weight ratio, tailorable characteristics, superior fatigue characteristics and damage tolerance compared to that of metals. Helicopter rotor blades, which play a dominant role in the overall vehicle performance, are typically made of composites. Deterministic design and analysis of composite structures use the nominal material properties of composites. However, effective material properties of composites are uncertain in nature because of the variations associated with the fiber and matrix material properties, fiber volume ratio, ply orientation, fiber waviness or undulation, voids, incomplete curing of resin, excess resin between plies, and variation in ply thickness [23,32]. It has been reported in the literature that the coefficients of variation (COV) of effective elastic moduli of a lamina can be 5–15 percent [23]. Thus the consideration of randomness in material properties is very important for the reliable analysis and design of composite aircraft structures. Further, the helicopter rotor system operates in a highly unsteady aerodynamic environment leading to severe vibratory loads [14]. Repeated exposure to this severe loading condition can deteriorate the structural characteristics of composite rotor blades. Therefore, the variations associated with the material and structural properties of composite rotor blade have to be considered in the aeroelastic analysis and designs.

Uncertainty quantification has emerged as a key issue in aeroelasticity [5,6,13,17,18,25,26,36]. Pettit [25] reviewed uncertainty quantification in aeroelasticity. Poirion [26] discussed some of the stochastic methods applied to aeroservoelasticity. Lindsley et al. [17] studied the effect of material uncertainty and boundary conditions on the non-linear aeroelastic response of panels. The effect of uncertainties in structural and aerodynamic parameters, modeled as random variables, on the dynamic instabilities of a two-dimensional rigid airfoil undergoing pitch and plunge motions has been studied by many researchers [5,13,36]. In the rotary wing field, Murugan et al. [19,20,29] studied the effects of uncertain material properties on the aeroelastic response predictions of composite helicopter rotors. The aeroelastic response of helicopter rotor blades has shown significant scatter from the baseline values due to material uncertainty. Murugan et al. [19,20] assumed the effects of randomness in material properties to be uniform throughout the span of the rotor blade. However, composite material properties can vary considerably along the span of the blade [17,32]. Sriramula and Chryssanthopoulos [32] reviewed studies that considered spatial variability in vibration, buckling and reliability problems of composite structures. Therefore, it is important to study the ef-

* Corresponding author. Tel.: +44 (0) 1792 602969, fax: +44 (0) 1792 295676.
E-mail address: s.m.masanam@swansea.ac.uk (S. Murugan).

1270-9638/$ – see front matter
doi:10.1016/j.ast.2011.02.004

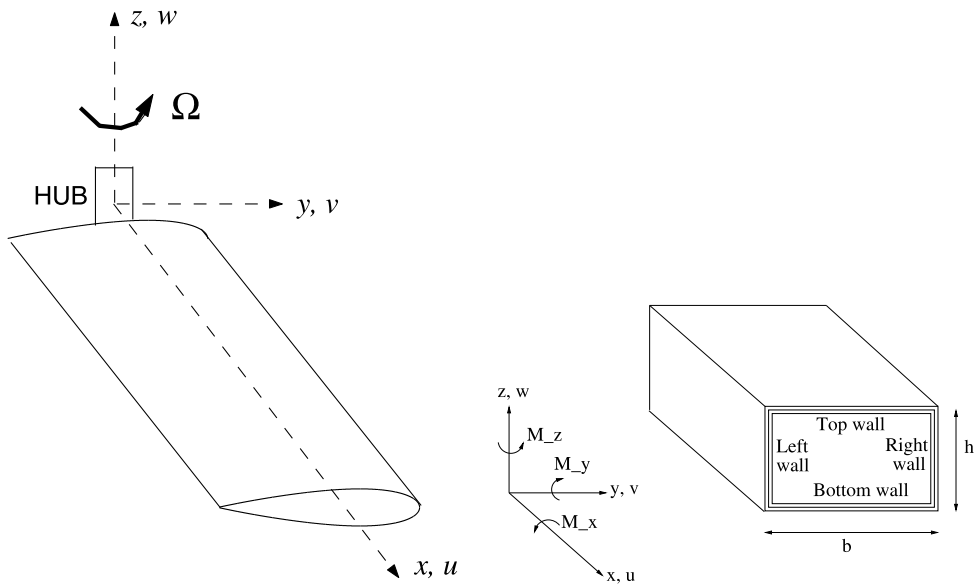

(a) Elastic rotor blade. (b) Composite box beam.

Fig. 1. Composite helicopter rotor blade.

fects of spatially uncertain material properties on the aeroelastic response predictions of rotor blade and this is the aim of this study.

Stochastic aeroelastic analyses are, generally, performed with direct Monte Carlo simulations which are computationally expensive [1,19,20]. Response surface methods and polynomial chaos expansion are proposed as computationally efficient methods to study the effect of parametric uncertainties, modeled as random variables, on the aeroelastic response [1,6,13]. However, there are no studies focused on developing a non-intrusive uncertainty analysis method to study the effects of spatial uncertainties on the aeroelastic response. This paper presents a generic approach to solve random field problems arising in structural mechanics. The proposed methodology uses the Karhunen–Loève (K-L) expansion [34] to discretize the input random field and high-dimensional model representation (HDMR) [27] to approximate the output response in terms of functions of lower dimensions as an efficient uncertainty propagation model. Compared to conventional surrogate models, the present approach has several advantages. First is the reduction in data processing. The exponentially growing number of function evaluations is represented via polynomially growing tables [8,16] for each function component (terms in the general expansion). This property improves the computational efficiency for high-dimensional real world problems. The second advantage is the reduction of computational complexity. HDMR is generated by a family of projection operators [27]. Consequently, the method splits any problem into easier low-dimensional subproblems. The third advantage is that HDMR is a mean-square convergent series expansion, because of the inherent orthogonal properties of HDMR component functions [27]. Also the lower-dimensional functions stay stable as higher-order Taylor series terms are inherently included. Finally, compared to existing simulation-based random field approaches [33], the HDMR-based approach does not translate into a lower-order polynomial approximation of system response. The formulation of the extended HDMR is similar to the spectral stochastic finite element method in the sense that both utilize the K-L expansion to represent the input, and a lower-order expansion to represent the output.

The approach discussed above decouples the computationally expensive aeroelastic simulations and the stochastic analysis. Spatial uncertainty analysis is performed with direct MCS and MCS based on HDMR models in this study. Numerical results from the HDMR models are compared with direct MCS and the effects of spatial uncertainty on helicopter aeroelastic response are studied. The helicopter aeroelastic model and HDMR models used in this study are discussed in the following sections.

2. Helicopter aeroelastic model

A comprehensive aeroelastic analysis code, UMARC, based on the finite element method, is used to evaluate the helicopter blade response [4]. UMARC has been extensively used by industry and academia for helicopter aeroelastic response predictions [11,35]. The aeroelastic formulation is briefly given in the following. The helicopter is modeled as a non-linear representation of composite rotor blades coupled to a rigid fuselage with 6-degrees of freedom. The rotor blade is modeled as a slender elastic beam undergoing flap bending displacement (w), lag bending displacement (v), elastic twist (ϕ), and axial deflection (u) with a rotational speed of Ω as shown in Fig. 1(a). The effect of moderate deflections is included by retaining second-order non-linear terms. For a given blade, the governing equations are derived using a generalized Hamilton's principle applicable to non-conservative systems:

$$\int_{\psi_1}^{\psi_2} (\delta U - \delta T - \delta W)\, d\psi = 0 \tag{1}$$

Here, δU is the virtual strain energy and δT is the virtual kinetic energy of the elastic blade. Also, δW is the virtual work done by the external aerodynamic forces acting on the blade and $\psi = \Omega t$ is the azimuth angle of the blade around the rotor disk. The Leishman–Beddoes unsteady aerodynamic model with the Bagai and Leishman free wake model is used for aerodynamic load calculations [4]. The blade is discretized into beam finite elements, each with fifteen degrees of freedom. These degrees of freedom correspond to cubic variations in axial and bending (flap and lag) deflections, and quadratic variation in elastic torsion. The finite element equations are reduced in size by using normal mode transformation. This results in the system of non-linear ordinary differential equation with periodic coefficients given below.

$$\mathbf{M}\ddot{\mathbf{p}}(\psi) + \mathbf{C}(\psi)\dot{\mathbf{p}}(\psi) + \mathbf{K}(\psi)\mathbf{p}(\psi) = \mathbf{F}(\mathbf{p}, \dot{\mathbf{p}}, \psi) \tag{2}$$

Here **M**, **C**, **K**, **F**, and **p** represent the finite element mass matrix, damping matrix, structural stiffness matrix, finite element force vector, and modal displacement vector, respectively. Non-linearities in the model occur primarily due to Coriolis terms and due to moderate deflections in the strain–displacement relations. Eq. (2) governs the dynamics of the rotor blade. These equations are then solved using the finite element in time method in combination with the Newton–Raphson method. The solution to these equations are then used to calculate rotor blade loads using the force summation method where aerodynamic forces are added to the inertial forces. The blade loads are integrated over the blade length and transformed to the fixed frame to estimate hub loads. The steady hub loads are then used to obtain the forces acting on the rotor and combined with fuselage and tail rotor forces to obtain the helicopter rotor trim equations:

$$\mathcal{F}_{\mathcal{T}}(\Theta_T) = \mathbf{0} \tag{3}$$

Here, the symbol Θ_T represents the flight control angles evaluated in the trim process [14]. These non-linear trim equations are also solved using the Newton–Raphson method. The helicopter rotor trim equations and the blade response equations in (2) and (3) are solved simultaneously to obtain the blade steady response and hub loads. This coupled solution procedure is important to capture the aeroelastic interaction between the aerodynamic forces and the blade deformations. Further details of the aeroelastic analysis are available in the UMARC theory manual [4].

3. Random field discretization

The random field representation and its discretization of spatial uncertainty is discussed in this section. A random field over ε is formally defined as an indexed set of random variables $\{\kappa_x(\theta)\}_{x\in\Omega}$, where $\kappa_x(\theta)$ are random variables with values in ε, defined on a probability space $(\Theta, \mathcal{B}, P)$. It should be noted that a probability space consists of three parts: (i) a sample space, Θ, which is the set of all possible outcomes; (ii) a set of events, where each event is a set containing zero or more outcomes (the collection of all such events is a σ-algebra $\mathcal{B}$); and (iii) the assignment of probabilities to the events, that is, a function from events to probability levels, using the probability measure function, P. Ω can be a finite or countable set, in which case the stochastic process is called a discrete stochastic process, or an uncountable set such as an interval $\Omega \subset \mathbb{R}$ or even a domain $\Omega \subset \mathbb{R}^d$. In the case where Ω is a spatial domain, the random process is called a random field. A stochastic process can be equivalently seen as a measurable function

$$\kappa : (x, \theta) \in \Omega \times \Theta \mapsto \kappa(x, \theta) \in \varepsilon \tag{4}$$

or alternatively as a random variable with values in a space of functions defined on Ω with values in ε. The equivalence between these different interpretations requires some technical considerations. In the following, one restricts the presentation to scalar random processes, i.e. $\varepsilon = \mathbb{R}$.

The characterization of a random process then requires the probabilistic characterization of a set of random variables, eventually uncountable. In fact, a random process can be completely characterized by its finite-dimensional probability laws, which are the joint probability laws of all finite sets of random variables $\{\kappa_{x_1}(\theta), \ldots, \kappa_{x_n}(\theta)\}$, $n \in \mathbb{N}, x_i \in \Omega$. Moreover, the random process is homogeneous if its mean $\mu(x, \theta)$ and variance $\sigma^2(x, \theta)$ are constant and its autocorrelation coefficient $\rho(x, x')$ is a function of $x - x'$ only. This autocorrelation function may take many distinct forms. One such form is the exponential type,

$$\rho(x, x') = e^{-\alpha_1 |x_{(1)} - x'_{(1)}| - \alpha_2 |x_{(2)} - x'_{(2)}|} \tag{5}$$

where $x_{(i)}$ denotes the ith coordinate of x and α_1, α_2 are known as correlation lengths.

In the following, we consider the representation and discretization of second-order processes. A wide variety of discretization schemes are available in the literature. The discretization methods can be divided into three groups [7,22,33]: point discretization (e.g., midpoint method, shape function method, integration point method, optimal linear estimate method), average discretization method (e.g., spatial average, weighted integral method) and series expansion method (e.g., Karhunen–Loève (K-L) expansion, polynomial chaos decomposition, orthogonal series expansion, expansion optimal linear estimation). Here we present the Karhunen–Loève (K-L) decomposition which is classically used in the context of spectral stochastic methods.

K-L decomposition [22] applies to second-order stochastic processes $\kappa \in L^2(\Omega) \otimes L^2(\Theta, dP)$. The random process $\kappa(x, \theta)$ is decomposed in the form:

$$\kappa(x, \theta) = \bar{\kappa}(x) + \sum_{i=1}^{\infty} \sqrt{\lambda_i}\psi_i(x)\zeta_i(\theta) \tag{6}$$

where $\bar{\kappa}(x)$ is the mean value of $\kappa(x, \theta)$, the functions $\psi_i(x)$ form a particular Hilbertian basis of $L^2(\Omega)$, $\zeta_i \in L^2(\Theta, dP)$ are centered uncorrelated random variables with unit variance and λ_i are positive constants. Couples $(\psi_i, \lambda_i) \in L^2(\Omega) \times \mathbb{R}^+$ are solutions of the eigenproblem

$$\int_{\Omega} \Gamma_\kappa(x, x')\psi_i(x')\,dx' = \lambda_i\psi_i(x) \tag{7}$$

where Γ_κ is the covariance function of $\kappa(x, \theta)$, defined by

$$\Gamma_\kappa(x, y) = E\big[\big(\kappa(x, \theta) - \bar{\kappa}(x)\big)\big(\kappa(x', \theta) - \bar{\kappa}(x')\big)\big] \tag{8}$$

In practice, the infinite series in Eq. (6) must be truncated, yielding a truncated K-L approximation

$$\tilde{\kappa}(x, \theta) = \bar{\kappa}(x) + \sum_{i=1}^{P} \sqrt{\lambda_i}\psi_i(x)\zeta_i(\theta) \tag{9}$$

which approaches $\kappa(x, \theta)$ in the mean-square sense as the positive integer $P \to \infty$. FE methods can be readily applied to obtain eigensolutions of any covariance function and domain of the random field. For linear or exponential covariance functions and simple domains, the eigensolutions can be evaluated analytically. According to Eq. (9), the K-L approximation provides a parametric representation of $\kappa(x, \theta)$ and, hence, of $\tilde{\kappa}(x, \theta)$ with P random variables. Note that this is not the only available technique to discretize the random field $\kappa(x, \theta)$. The K-L expansion has uniqueness and error-minimization properties that make it a convenient choice over other available methods. Generally speaking, if $\zeta_i(\theta)$ contains non-Gaussian random variables, then it is difficult to obtain a representation in independent random variables, as un-correlation and independence are not equivalent. Obtaining a representation in independent random variables for a non-Gaussian field $\kappa(x, \theta)$ usually involves non-linear transformations of the random variables [2,3,21].

4. High-dimensional model representation (HDMR)

The high-dimensional model representation (HDMR) of an arbitrary M-dimensional response $f(\mathbf{x})$, $\mathbf{x} \in \Re^M$ can be derived by partitioning the identity operator $\mathcal{I}$, called $\mathcal{I}_M$ in the M-dimensional case and also in the 1D case hereafter, with respect to the projectors $\mathcal{P}_1, \mathcal{P}_2, \ldots, \mathcal{P}_M$. This can be expressed as [27]

$$\begin{aligned}\mathcal{I}_M &= \prod_{m=1}^{M}\left(\mathcal{P}_m + (\mathcal{I}_1 - \mathcal{P}_m)\right)\\ &= \underbrace{\prod_{m=1}^{M}\mathcal{P}_m}_{1\text{ term}} + \underbrace{\sum_{m=1}^{M}(\mathcal{I}_1 - \mathcal{P}_m)\prod_{s\neq m}\mathcal{P}_s}_{\binom{M}{1}\text{ terms}}\\ &\quad + \underbrace{\sum_{m=1}^{M}\sum_{s=m+1}^{M}(\mathcal{I}_1 - \mathcal{P}_m)(\mathcal{I}_1 - \mathcal{P}_s)\prod_{p\neq m,s}\mathcal{P}_p}_{\binom{M}{2}\text{ terms}}\\ &\quad + \cdots + \underbrace{\sum_{m=1}^{M}\mathcal{P}_m\prod_{s\neq m}(\mathcal{I}_1 - \mathcal{P}_s)}_{\binom{M}{M-1}\text{ terms}} + \underbrace{\prod_{m=1}^{M}(\mathcal{I}_1 - \mathcal{P}_m)}_{1\text{ term}} \end{aligned} \tag{10}$$

which is composed of 2^M mutually orthogonal terms and $\mathcal{P}_m(\mathcal{I}_1 - \mathcal{P}_m) = 0$. The orthogonal representation of Eq. (10) is a manifestation of the HDMR and can be rewritten as [15,28],

$$\begin{aligned} f(\mathbf{x}) &= f_0 + \sum_{i=1}^{M} f_i(x_i)\\ &\quad + \sum_{1\leqslant i<j\leqslant M} f_{ij}(x_i, x_j) + \cdots + f_{123\ldots M}(x_i, x_2, \ldots, x_M)\\ &= \sum_{l=0}^{M}\eta_l(\mathbf{x}) \end{aligned} \tag{11}$$

where f_0 is a constant term representing the zeroth-order component function or the mean response of output function $f(\mathbf{x})$. f_i is the first-order term expressing the effect of variable x_i acting alone upon the output $f(\mathbf{x})$, and this function is generally non-linear. The function $f_{ij}(x_i, x_j)$ is a second-order term which describes the cooperative effects of the variables x_i and x_j upon the response. The higher-order terms give the cooperative effects of increasing numbers of input variables acting together to influence the output. The last term $f_{123\ldots M}(x_i, x_2, \ldots, x_M)$ contains any residual dependence of all the input variables locked together in a cooperative way to influence the output. Once all of the relevant component functions in Eq. (11) are determined and suitably represented, then the component functions constitute the HDMR, thereby replacing the original computationally expensive method of calculating the response by the computationally efficient meta model. Usually the higher-order terms in Eq. (11) are negligible [10,15] such that an HDMR with only a few low-order correlations amongst the input variables is adequate to describe the output behavior. This in turn results in rapid convergence of the HDMR expansion [30], which has a finite number of terms and is always exact [15] in the least-square senses. Other popular expansions (e.g., polynomial chaos) have been suggested [12], but they commonly have an infinite number of terms with some specified functions, such as Hermite polynomials [27].

To generate the HDMR approximation of any function, more precisely the cut-center-based HDMR, first a reference point $\bar{\mathbf{x}} = (\bar{x}_1, \bar{x}_2, \ldots, \bar{x}_M)$ has to be defined in the variable space. In the convergence limit, where all correlated functions in Eq. (11) are considered, the cut-HDMR is invariant to the choice of reference point $\bar{\mathbf{x}}$. However in practice the choice of reference point $\bar{\mathbf{x}}$ is important for the cut-HDMR, especially if only the first few terms, say up to first- and second-order, in Eq. (11) are considered. Sobol [30] showed that the reference point $\bar{\mathbf{x}}$ at the middle of the input domain appears to be the optimal choice. The expansion functions are determined by evaluating the input–output responses of the system relative to the defined reference point in the input variable space. This process reduces to the following relationship for the component functions in Eq. (11):

$$\begin{aligned} f_0 &= \int dx\, f(\mathbf{x})\\ f_i(x_i) &= \int dx^i\, f(\mathbf{x}) - f_0\\ f_{ij}(x_i, x_j) &= \int dx^{ij}\, f(\mathbf{x}) - f_i(x_i) - f_j(x_j) - f_0 \end{aligned} \tag{12}$$

where $\int dx^i$ means to integrate over all M variables except x_i and $\int dx^{ij}$ means to integrate over all M variables except x_i and x_j, etc. These integrals are generally evaluated using numerical integration techniques. Substituting the component functions defined in Eq. (12) into Eq. (11), the general expression of the HDMR can be expressed as

$$\begin{aligned} f(\mathbf{x}) &= \sum_{1\leqslant i_1<\cdots<i_\beta\leqslant M} f\left(x_{i_1}, \ldots, x_{i_\beta}; \bar{x}^{i_1,\ldots,i_\beta}\right)\\ &\quad - (M-\beta)\sum_{1\leqslant i_1<\cdots<i_{\beta-1}\leqslant M} f\left(x_{i_1}, \ldots, x_{i_{\beta-1}}; \bar{x}^{i_1,\ldots,i_{\beta-1}}\right)\\ &\quad + \frac{(M-\beta+1)!}{2!(M-\beta-1)!}\\ &\quad \times \sum_{1\leqslant i_1<\cdots<i_{\beta-2}\leqslant M} f\left(x_{i_1}, \ldots, x_{i_{\beta-2}}; \bar{x}^{i_1,\ldots,i_{\beta-2}}\right) - \cdots\\ &\quad \mp \frac{(M-2)!}{(\beta-1)!(M-\beta-1)!}\sum_{1\leqslant i\leqslant M} f\left(x_i; \bar{x}^i\right)\\ &\quad \pm \frac{(M-1)!}{\beta!(M-\beta-1)!} f(\bar{\mathbf{x}}) \end{aligned} \tag{13}$$

where β is the order of the HDMR approximation, $1 \leqslant \beta \leqslant (M-1)$ and the $+$ or $-$ sign of the last term in Eq. (13) corresponds to β being even or odd, respectively. Considering the weak role of the higher-order correlation effects, the approximation is likely to converge at a lower HDMR order, say, $\beta \ll M$. The particular form of Eq. (13) for $\beta = 1$, 2 or 3 corresponds to first-, second- or third-order HDMR can be explicitly given as

$$\hat{f}(\mathbf{x}) = \sum_{1\leqslant i\leqslant M} f\left(x_i; \bar{x}^i\right) - (M-1) f(\bar{\mathbf{x}}), \quad \beta = 1 \tag{14}$$

$$\begin{aligned} \hat{f}(\mathbf{x}) &= \sum_{1\leqslant i<j\leqslant M} f\left(x_i, x_j; \bar{x}^{i,j}\right) - (M-2)\sum_{1\leqslant i\leqslant M} f\left(x_i; \bar{x}^i\right)\\ &\quad + \frac{(M-1)!}{2!(M-3)!} f(\bar{\mathbf{x}}), \quad \beta = 2 \end{aligned} \tag{15}$$

$$\begin{aligned} \hat{f}(\mathbf{x}) &= \sum_{1\leqslant i<j<k\leqslant M} f\left(x_i, x_j, x_k; \bar{x}^{i,j,k}\right)\\ &\quad - (M-3)\sum_{1\leqslant i<j\leqslant M} f\left(x_i, x_j; \bar{x}^{i,j}\right)\\ &\quad + \frac{(M-2)!}{2!(M-4)!}\sum_{1\leqslant i\leqslant M} f\left(x_i; \bar{x}^i\right)\\ &\quad + \frac{(M-1)!}{3!(M-4)!} f(\bar{\mathbf{x}}), \quad \beta = 3 \end{aligned} \tag{16}$$

The term $f(x_i; \bar{x}^i)$ is a function of the single x_i component (i.e., a cut along x_i through the reference point in the function space), while the other variables, $x_j \equiv \bar{x}_j$, $j \neq i$, are fixed at the reference

point. In the same manner, $f(x_i, x_j; \bar{x}^{i,j})$ is the observed response for all the variables, $x_k \equiv \bar{x}_k$, $k \neq i, j$, fixed at the cut center except for x_i and x_j. A similar interpretation would apply to higher-order HDMR terms.

The notion of first, second order, etc. used in the HDMR does not imply the terminology commonly used either in the Taylor series or in the conventional polynomial-based approximation formulae. In HDMR-based approximation, these terminologies are used to define the constant term, terms with one variable or two variables only. It is recognized that the lower-order (e.g., first-order or second-order) function expansions in the HDMR, do not generally translate to linear or quadratic functions [10]. Each of the lower-order terms in the HDMR is sub-dimensional, but they are not necessarily low degree polynomials. The computational savings afforded by the HDMR are easily estimated. If the HDMR converges at β order with acceptable accuracy and considering s sample points for each variable, then the total number of numerical analyses needed to determine the HDMR is $\sum_{k=0}^{\beta}[M!/k!(M-k)!](s-1)^k$.

5. Numerical results

The effects of spatial uncertainty on the rotating natural frequencies and vibratory hub loads of a composite hingeless helicopter rotor are studied in this section. The rotor blade is considered as a uniform blade equivalent of the BO-105 rotor blade and its properties are given in Table 1. The cross-section of rotor blade is modeled as a composite box beam with a breadth of 0.144 m, and height of 0.081 m as shown in Fig. 1(b). All the four walls of box beam are considered to be made of a laminate with stacking sequence of $[0_3/\pm 15_3/\pm 45_2]_s$. Each wall of the box beam is therefore made of a balanced symmetric laminate with 26 plies of graphite/epoxy material, where each ply is 0.127 mm thick. The box-beam type representation of the rotor blade is extensively used in rotorcraft aeroelastic analysis and optimization studies [19,31]. Initially, a baseline analysis is carried out with the nominal material properties and the results of uncertainty analysis are compared with these baseline results.

Most studies on uncertainty analysis of composite structures consider E_1, E_2, G_{12} and ν_{12} as statistically independent random variables [23]. In this study, the composite material properties, E_1, E_2, G_{12} and ν_{12}, are considered as independent random variables with normal distributions. The COVs for each of the above material properties are taken from Ref. [23] and listed in Table 2. Initially, the effects of uncertain material properties on the cross-sectional stiffnesses such as flap bending (EI_y), lag bending (EI_z) and torsional stiffness (GJ) of rotor blade are evaluated. With the statistical measures of uncertainty in cross-sectional stiffness, the spatial variations of stiffness properties along the blade span are modeled. In the first stage, as a preliminary study, the stiffness properties of each beam element are considered as independent discrete random variables to represent spatial uncertainty of rotor blade and the uncertainty effects on rotating natural frequencies are studied with direct MCS. In the second stage, the stiffness properties are considered to be spatially varying along the axis of the blade (ξ), as an independent, homogeneous, log-normal random fields. That is, the torsional stiffness $GJ(\xi)$ is given as $c_1 \exp[\alpha_1(\xi)]$, bending stiffnesses, $EI_y(\xi)$ as $c_2 \exp[\alpha_2(\xi)]$ and $EI_z(\xi)$ as $c_2 \exp[\alpha_2(\xi)]$. HDMR models are developed to approximate the aeroelastic outputs in terms of the blade stiffnesses as random fields. The effects of uncertainty on the vibratory hub load predictions are studied with MCS based on HDMR models. The analysis and results of these two stages are discussed in the following sections.

Table 1
Baseline hingeless rotor blade properties.

Number of blades	4
Radius, R (m)	4.94
Hover tip speed, ΩR (m/s)	198.12
Mass per unit length, m_o (kg/m)	6.46
Lock number	6.34
Solidity	0.10
C_T/σ	0.07

Table 2
Scatter in material properties.

Material properties	Mean	COV (%)
E_1 (GPa)	141.96	7.0
E_2 (GPa)	9.79	4.0
G_{12} (GPa)	6.00	11.0
ν_{12}	0.42	4.0

Table 3
Statistics of cross-sectional stiffness values.

Stiffness (non-dimensional)	Baseline value	COV (%)
$GJ/m_o\Omega^2R^4$	0.003817	6.04
$EI_y/m_o\Omega^2R^4$	0.008335	6.51
$EI_z/m_o\Omega^2R^4$	0.023174	6.51

5.1. Effects of spatial uncertainty on blade frequencies

Uncertainty effects on the blade cross-sectional stiffnesses are evaluated with 5000 random samples of material properties with the COVs listed in Table 2 [19]. With these random material properties, the flap bending, lag bending and torsional stiffnesses of rotor blade show COVs of 6.51, 6.51 and 6.04 percent, respectively, as given in Table 3. Such a large uncertainty can cause considerable changes in dynamic response predictions.

The variations of the stiffness properties along the axis of rotor blade are now modeled with the above uncertainty results. The rotor blade is divided into 10 beam elements and the cross-sectional stiffnesses of each beam element are considered as discrete random variables with COVs given in Table 3. The spatial variations of stiffnesses of each beam element are shown in Fig. 2; in the later section of this paper, random fields are used to approximate the spatial variations. Uncertainty effects on the rotating natural frequencies of rotor blade are studied with direct MCS.

MCS is performed with 1000 samples and the results for the rotating frequencies are given in Table 4. An additional MCS is performed by assuming the stiffness properties of all beam elements of the rotor blade have the same level of uncertainty and these results are also given in Table 4. This comparison of results highlights the difference between spatial uncertainty and considering only material uncertainty. Fundamental flap, lag and torsion bending frequencies show COVs of 0.28, 1.24 and 1.06% for spatially varying stiffness properties. However, the fundamental frequencies show COVs of 0.42, 2.29 and 3.05% when considering spatially uniform uncertain stiffness properties. The effect of spatial uncertainty is significantly different from the effect of uniform uncertainty along the span. The effects of spatial uncertainty are considerably less than the uniform variation case which can be expected due to averaging of spatial variations. Another interesting result is that uncertainty effects on rotating frequencies increase monotonically with the higher modes of flap, lag and torsion motion in the uniform variation case. However, the COVs of the frequencies do not vary monotonically with the higher modes for lag and torsion motion in the spatially varying case. For example, the first four lag modes show COVs of 2.29, 2.47, 3.04 and 3.26 percent for the spa-

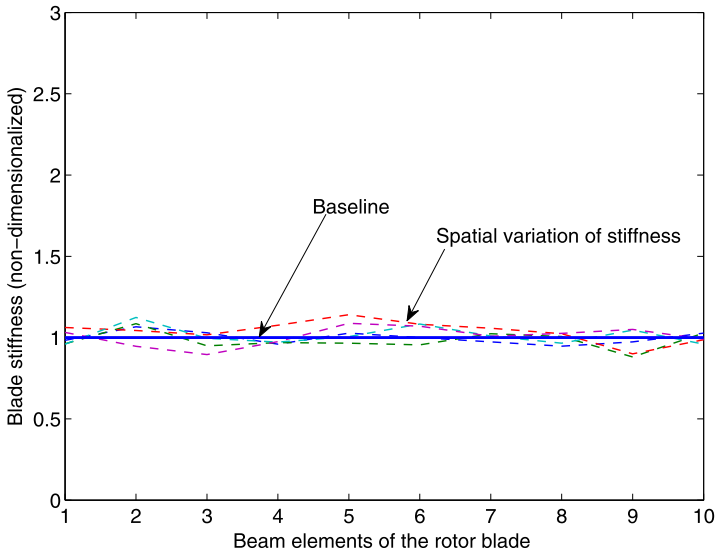

Fig. 2. Spatial variation of blade stiffness.

Table 4
Uncertainty effects on blade rotating frequencies.

Mode	Baseline (/rev) frequencies	COV (%)	
		Spatially uniform stiffness	Spatially uncertain stiffness
Flap 1	1.14	0.42	0.28
Flap 2	3.40	1.47	0.54
Flap 3	7.47	2.39	0.85
Flap 4	13.45	2.83	0.93
Lag 1	0.75	2.29	1.24
Lag 2	4.37	2.47	0.91
Lag 3	11.03	3.04	1.10
Lag 4	20.91	3.26	1.08
Torsion 1	4.58	3.05	1.06
Torsion 2	13.58	3.12	1.18
Torsion 3	22.62	3.13	1.10

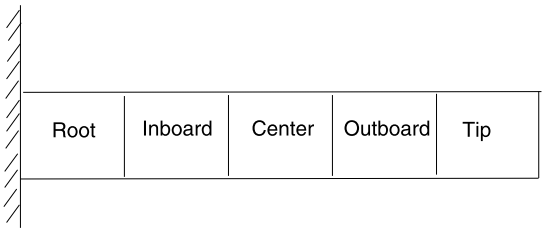

Fig. 3. Sections of rotor blade.

tially uniform stiffness case. The same four lag modes show COVs of 1.24, 0.91, 1.10 and 1.08 percent for the spatially varying case.

To study the effects of spatial uncertainty further, a sensitivity analysis is carried out. The uncertainty on the rotating frequencies corresponding to uncertainty at each section of the rotor blade is studied. Generally, the rotor blade is divided into root, inboard, center, outboard and tip sections along the blade span in structural health monitoring studies [24]. Similarly, in this study, the rotor blade is divided into five sections as shown in Fig. 3. The stiffness properties of each section are considered to be uncertain while the properties of the other sections are kept at their deterministic values. Each section shown in Fig. 3 consists of two beam elements. The effects of uncertainty on the rotating frequencies are evaluated with MCS based on 1000 samples. This results in 5000 simulations with each section having 1000 samples. The uncertainty effects on the first three modes of flap, lag and torsion motion are shown in Figs. 4(a)–4(c). The first modal frequencies of the flap, lag and torsion motions are sensitive to uncertainty in the root and inboard sections of the blade as shown in Fig. 4(a). Uncertain stiffness properties of the center, outboard and tip sections of the blade have a minor effect on the fundamental flap and lag frequencies whereas they have a significant influence on the fundamental torsion frequency. Fig. 4(b) shows that the second modal frequency of all three motions is more sensitive to the uncertain stiffness properties of root, center and outboard sections than the inboard and tip sections of blade. Similarly, the outboard and tip have a considerable influence on the third modal frequencies of the rotor blade as shown in Fig. 4(c). This study shows that the uncertainty at different sections of the rotor blade has varying levels of influence on the modal frequencies which is clearly related to mode shapes. Also, the first three modes of flap, lag and torsion motions are found to sufficiently capture the spatial uncertainty at all the sections of rotor blade.

The above uncertain free vibration analysis is performed with direct MCS. Uncertainty on rotating frequencies is studied with 1000 samples as the free vibration analysis involves only structural contributions. However, to study the effects on aeroelastic response which involve structural and aerodynamic interactions, direct MCS with a computational aeroelastic code can be expensive for a sufficient number of samples. Therefore, an approximation method to replace the computational aeroelastic model is developed in the next section.

5.2. HDMR of aeroelastic model

The HDMR models to approximate the aeroelastic response are discussed in this section. Based on the theory discussed in Sections 3 and 4, the proposed methodology for the HDMR approximation is implemented using the following steps:

1. Represent the random field inputs in terms of standard random variables by a K-L expansion.
2. Select the reference point $\bar{\mathbf{x}}$, generally as the mean of the input variables.
3. Determine f_0, which is a constant term, representing the response at reference point $\bar{\mathbf{x}}$.
4. Generate regularly spaced sample points for each variable, as $x_i^1 = \bar{x}_i - (s-1)k_i/2, x_i^2 = \bar{x}_i - (s-3)k_i/2, \ldots, x_i^{(s+1)/2} = \bar{x}_i, \ldots, x_i^{s-1} = \bar{x}_i + (s-3)k_i/2$, $x_i^s = \bar{x}_i + (s-1)k_i/2$, along the

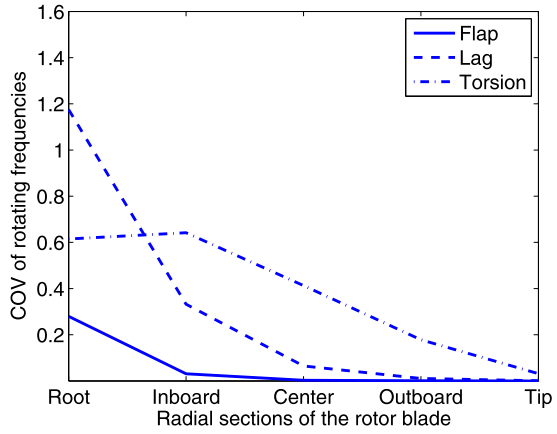

(a) First modal frequency

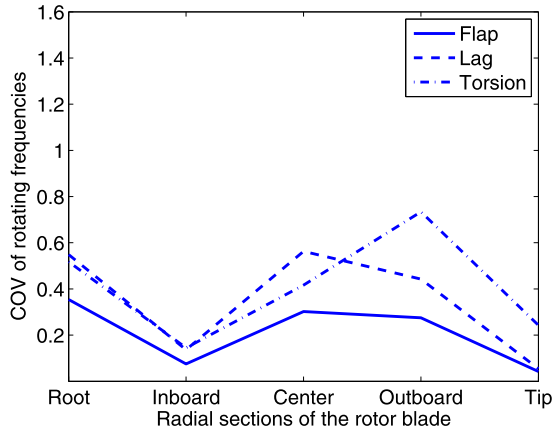

(b) Second modal frequency

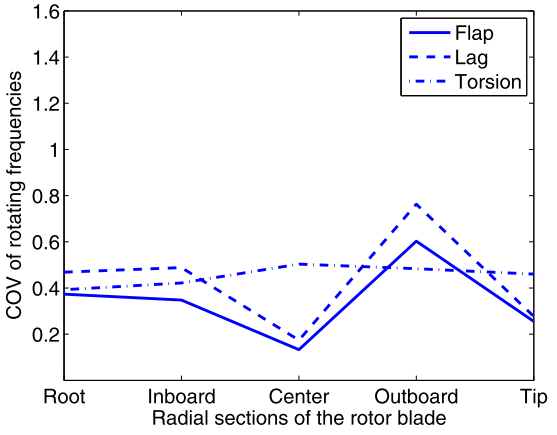

(c) Third modal frequency

Fig. 4. Sensitivity of modal frequencies to spatial uncertainty of rotor blade.

variable axis x_i with reference $\bar{x}_i$ and regular spacing k_i, which is the standard deviation of x_i. Here, s denotes the number of HDMR sample points, and must be odd. More details about the choice of reference points and other details can be found in [28].

5. Estimate the responses at the sample points for each variable using the computational model.
6. Construct the HDMR approximation using following steps:
   - Interpolate each of the low-dimensional (e.g., first-order) HDMR expansion terms $f(x_i;\bar{x}^i)$ as $f(x_i;\bar{x}^i) = \sum_{j=1}^{s} \varphi_j(x_i) \times f(x_i^j;\bar{x}^i)$. The response values are calculated in previous step and $\varphi_j(x_i)$ represents interpolation/shape functions. In this study, moving least-square interpolation functions are used and the details of which can be found in Ref. [9].
   - Sum the interpolated values of HDMR expansion terms. This leads to the first-order HDMR approximation of the function $f(\mathbf{x})$ as follows:

$$\hat{f}(\mathbf{x}) = \sum_{1\leqslant i\leqslant M} \sum_{j=1}^{s} \varphi_j(x_i) f\left(x_i^j;\bar{x}^i\right) - (M-1) f(\bar{\mathbf{x}}), \quad \beta = 1 \tag{17}$$

7. Perform Monte Carlo simulations using the approximated response function $\hat{f}(\mathbf{x})$.
8. Estimate the output statistics.

Numerical parameters of the above steps are discussed here. Normalized mean and COVs of the random fields (i.e., flap bending, lag bending and torsional stiffness) are $\mu_{GJ} = 1.0$, $\mu_{EI_y} = 1.0$, $\mu_{EI_z} = 1.0$; and $\upsilon_{GJ} = 0.060$, $\upsilon_{EI_y} = 0.065$, $\upsilon_{EI_z} = 0.065$, respectively. $c_1 = \mu_{GJ}/\sqrt{1+\upsilon_{GJ}^2}$, $c_2 = \mu_{EI_{y,z}}/\sqrt{1+\upsilon_{EI_{y,z}}^2}$ and $\alpha_1(\xi)$, $\alpha_2(\xi)$ are zero-mean, homogeneous, Gaussian random fields. The variance and covariance functions of the random fields are $\sigma_{\alpha_1}^2 = \ln(1+\upsilon_{GJ}^2)$, $\sigma_{\alpha_2}^2 = \ln(1+\upsilon_{EI_{y,z}}^2)$ and $\Gamma_{\alpha_1}(\xi_1,\xi_2) = \sigma_{\alpha_1}^2 \exp(-|\xi_1 - \xi_2|/b)$, $\Gamma_{\alpha_2}(\xi_1,\xi_2) = \sigma_{\alpha_2}^2 \exp(-|\xi_1 - \xi_2|/b)$, respectively. b is the correlation parameter that controls the rate at which the covariance decays. The degree of variability associated with the random process can be related to its coefficient of variation. The frequency content of the random field is related to the L/b ratio in which L is the length of the blade. $L/b = 0.5$ is chosen in this study. In this example, the normalized length of the blade is $L = 1$ and it is divided into 10 elements.

The eigensolutions of the covariance function are obtained by solving the integral equation (Eq. (7)) analytically. The eigenvalues and eigenfunctions are given as follows:

$$\lambda_i = \frac{2\sigma_\alpha^2 b}{\omega_i^2 + b^2}$$

$$\lambda_i^* = \frac{2\sigma_\alpha^2 b}{\omega_i^{*2} + b^2}$$

$$\psi_i(\xi) = \frac{\cos(\omega_i \xi)}{\sqrt{a + \frac{\sin(2\omega_i \xi)}{2\omega_i}}} \quad \text{for } i = \text{odd}$$

$$\psi_i(\xi) = \frac{\sin(\omega_i^* \xi)}{\sqrt{a - \frac{\sin(2\omega_i^* \xi)}{2\omega_i^*}}} \quad \text{for } i = \text{even} \tag{18}$$

The symbol ω_i presents the period of the random field. The random field is discretized into ten standard random variables, and the ten-term K-L expansion (Eq. (9)) is used to generate sample functions of the input random field. Realizations of the cross-sectional stiffnesses of the blade are numerically simulated using the K-L expansion method. The response quantities of the blade are represented by HDMR expansion with seven sample points. Thus, total number of function evaluations ($(s-1)\times M + 1 = (7-1)\times 10 + 1$) required for HDMR is 61 (Fig. 5). It should be noted that, HDMR-based approach requires conditional responses at selected sample points and the sample points are chosen along each of the variable axis. A considerable number of engineering problems and non-linear mathematical functions with HDMR approximations have been studied by the authors in Refs. [7–9]. It is

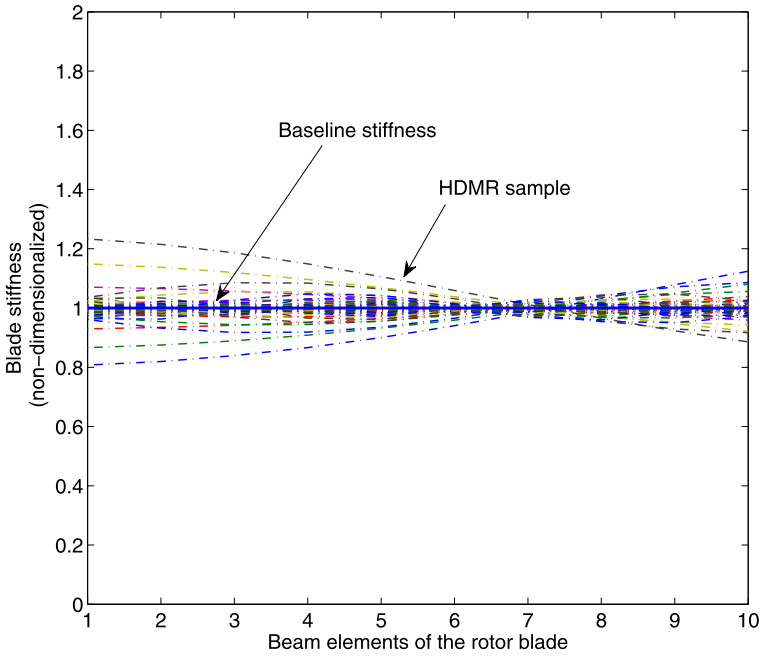

Fig. 5. Samples of uncertain stiffness for HDMR models.

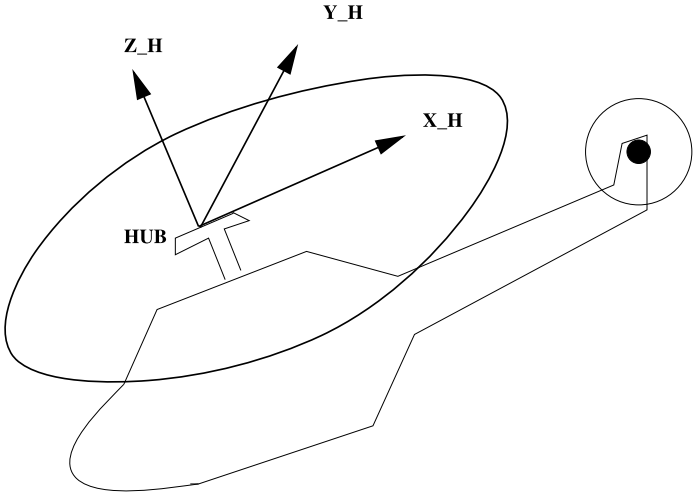

Fig. 6. Coordinate system of the rotor hub.

found from the authors' previous studies that $s = 5$ or 7 works well for most of the problem. Due to this fact, results for $s = 7$ are used in this paper to construct HDMR-based meta models.

5.3. Stochastic aeroelastic analysis with HDMR models

In helicopters, the aerodynamic loads acting on the rotor blades are transmitted to the fuselage and cause severe vibrations. For a rotor with N blades, the loads with frequencies that are integer multiples of $N\Omega$ are transmitted from rotor to the hub [14]. The prediction of these vibratory loads is a key issue in the aeroelastic analysis, design, and optimization of rotorcraft [11]. For a four bladed rotor considered in this study, the impact of spatial uncertainty on the 4/rev (per revolution) vibratory loads which are longitudinal shear (F_x), lateral shear (F_y), and vertical shear (F_z) along with the rolling moment (M_x), pitching moment (M_y), and yawing moment (M_z) are studied. Note, the vibratory hub loads ($F_x, F_y, F_z, M_x, M_y, M_z$) are associated with the coordinate system of the rotor hub shown in Fig. 6 [4]. The 4/rev forces are normalized by the rotor steady thrust and the 4/rev moments are normalized by the rotor steady yawing moment. The baseline values of vibratory hub loads, at an advance ratio of 0.3, are given in Figs. 7(a) and 7(b).

To evaluate the accuracy of the developed HDMR models, MCS with 1000 samples is performed with the HDMR models and the actual aeroelastic computational code, and the results are compared. COVs of the rotating frequencies from direct MCS and HDMR-based MCS are given in Table 5. Note, these uncertainty results of frequencies are different to those in Section 5.1 as the samples and spatial modeling of uncertainties are different. Table 5 shows that HDMR models are quite accurate, compared to the direct MCS, in predicting the COVs of the frequencies. Now the HDMR models of vibratory hub loads, which involve aeroelastic simulations, are compared to the direct simulation results. Probability distribution functions (PDF) of the vibratory hub force F_z and vibratory hub moment M_z from the direct MCS and HDMR-based MCS with 1000 samples are shown in Figs. 8(a) and 8(b), respectively. It is observed that the PDFs from MCS based on HDMR mod-

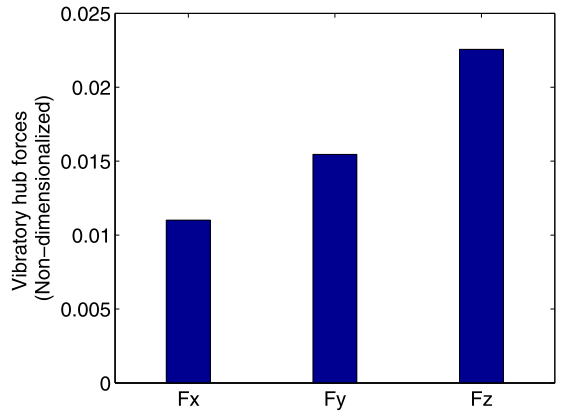

(a) Baseline vibratory forces at the rotor hub.

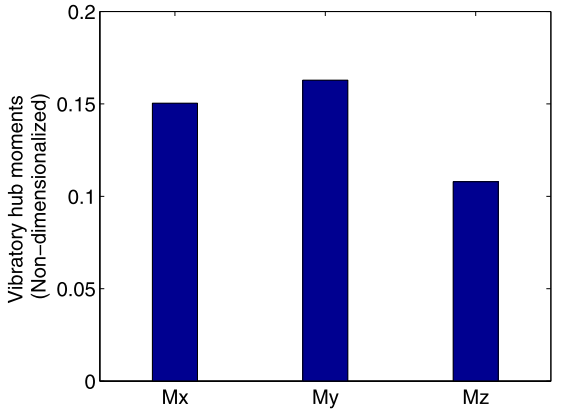

(b) Baseline vibratory moments at the rotor hub.

Fig. 7. Baseline vibratory forces and moments.

els are able to approximate, with reasonable accuracy, the PDFs from direct MCS.

The HDMR models are now used to evaluate the effects of the spatial uncertainty on the six vibratory hub loads with one hundred thousand samples. Note, the CPU time for the aeroelastic simulations with 1000 samples is approximately 10 CPU hours in a PC with quad core processor. Therefore, for one hundred thousand samples, it would take approximately 1000 CPU hours which is very expensive compared to MCS with HDMR models that takes only a few minutes. Further, the HDMR models are developed with 61 aeroelastic simulations which take approximately 1 CPU hour only. The PDFs of baseline vibratory forces and moments are shown in Figs. 9(a)–10(c). The longitudinal vibratory force shows a deviation of −20 to 20 percent from its baseline value, the lateral force shows a deviation of −5 to 10 percent, and the vertical force shows a deviation of −60 to 40 percent. The vertical vibratory force is dominant among all three forces, as shown in Fig. 7(a), and is highly sensitive to the uncertainties. The rolling and pitching moments show a scattering of around −2 to 1 percent from their baseline values. However, the vibratory yawing moment shows scattering of around −20 to 60 percent. Further, the PDFs of 4/rev loads given in Figs. 9(a) and 10(c) show non-Gaussian type distributions. The results from this study show that parametric uncertainty plays a major role in reliable aeroelastic predictions and have to be incorporated in the design and optimization of composite aircraft structures. For uncertainty analysis, the development of approximation models such as HDMR methods can reduce the computational cost of stochastic analysis.

Table 5
Uncertainty effects on blade rotating frequencies.

Mode	COV (%)	
	Direct MCS	MCS with HDMR
Flap 1	0.42	0.50
Flap 2	0.67	0.67
Lag 1	2.17	2.18
Lag 2	1.15	1.14
Torsion 1	2.22	2.20
Torsion 2	1.11	1.16

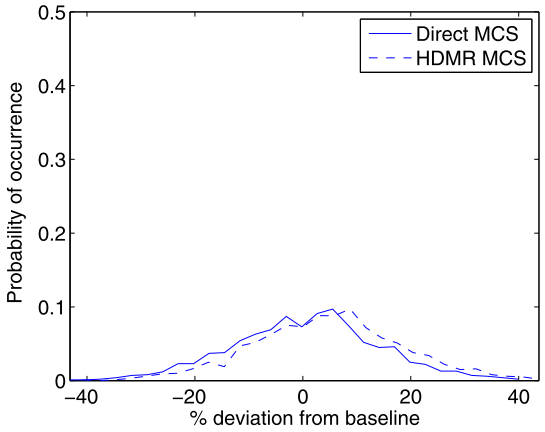

(a) Effects of spatial uncertainty on vibratory hub force, F_z.

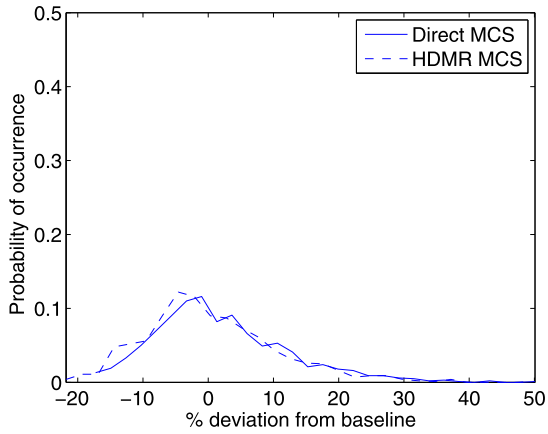

(b) Effects of spatial uncertainty on vibratory hub moment, M_z.

Fig. 8. Effects of spatial uncertainty on vibratory loads with direct MCS and HDMR-based MCS.

6. Conclusions

The effects of spatially uncertain rotor blade properties on the aeroelastic response of composite helicopter rotor have been studied. Initial results based on direct Monte Carlo simulation show the spatial uncertainty has considerable impact on aeroelastic response predictions. To reduce the computational cost of stochastic aeroelastic analysis, the high-dimensional model representation of the computational aeroelastic model is developed and Monte Carlo simulations are then performed with these developed models. The following conclusions are drawn from this study:

1. Uncertainty in the composite material properties has considerable influence on the rotating frequencies of rotor blades. The effects of spatially uncertain material properties, and thus the spatially uncertain stiffness properties of rotor blade, have ef-

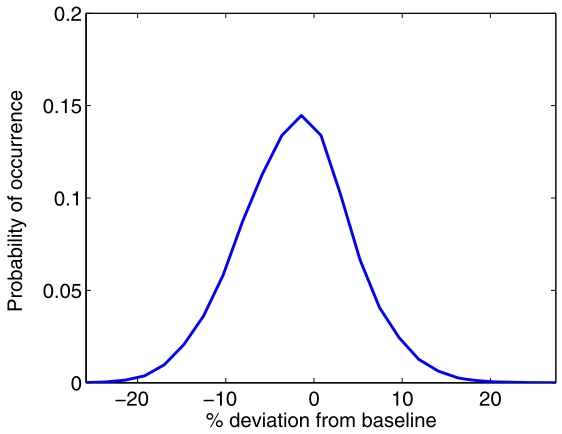

(a) Effects of spatial uncertainty on vibratory hub force, F_x.

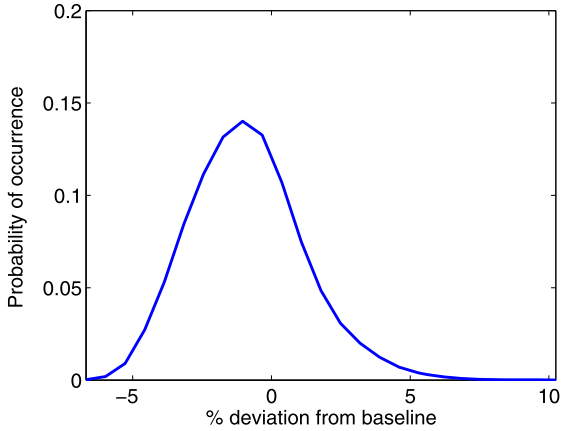

(b) Effects of spatial uncertainty on vibratory hub force, F_y.

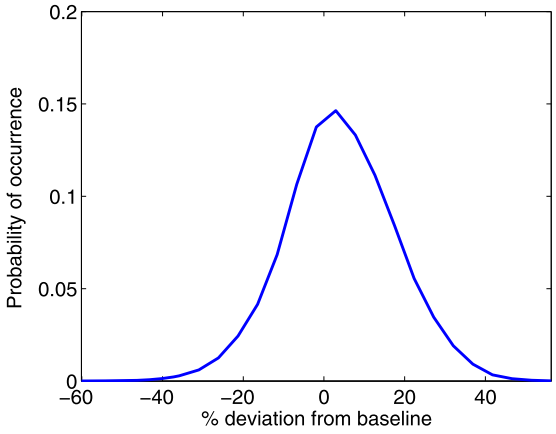

(c) Effects of spatial uncertainty on vibratory hub force, F_z.

Fig. 9. Effects of spatial uncertainty on vibratory forces with HDMR-based MCS.

fects that vary with the rotating frequencies, compared to the case of uniform material uncertainty.

2. Uncertainty effects on the rotating frequencies vary with the higher modes of flap, lag and torsion motion. The COVs of frequencies increase with the higher-order modes when material uncertainty is considered as spatially uniform. However, the COVs of rotating frequencies do not increase monotonically with higher-order modes in lag and torsion motion when spatially uncertain material properties are considered.

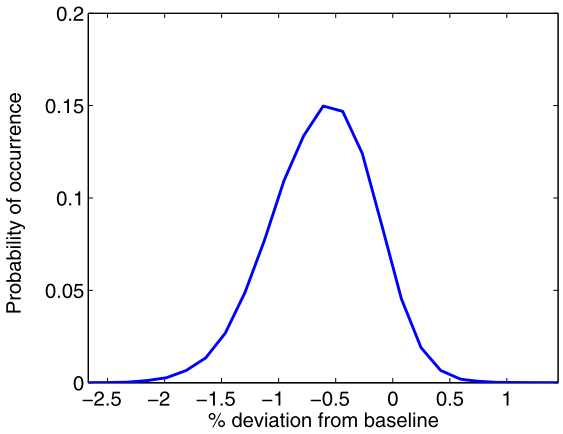

(a) Effects of spatial uncertainty on vibratory hub moment, M_x.

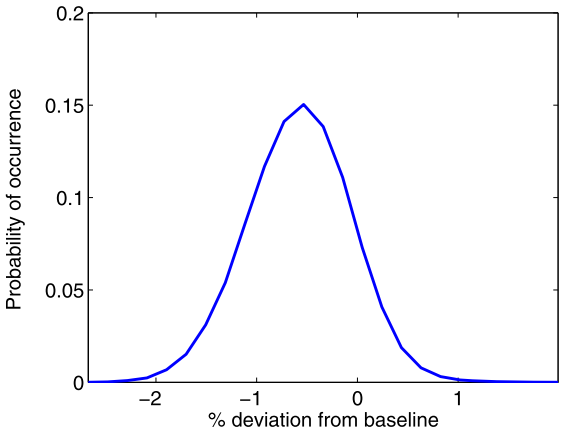

(b) Effects of spatial uncertainty on vibratory hub moment, M_y.

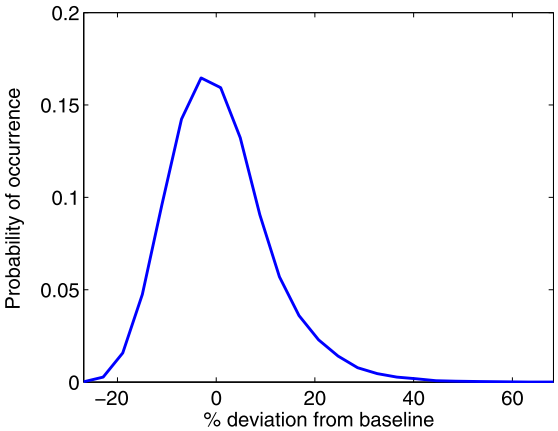

(c) Effects of spatial uncertainty on vibratory hub moment, M_z.

Fig. 10. Effects of spatial uncertainty on vibratory moments with HDMR-based MCS.

3. Fundamental frequencies of flap, lag and torsion are sensitive to uncertainty at the root and inboard sections of rotor blade. Second-order modes of flap, lag and torsion are sensitive to the center and outboard sections. Uncertainties at the outboard and tip sections of blade have considerable influence on the third-order modes but not on the first- and second-. Also,

the first mode seems to reasonably capture the spatial uncertainties at each section of the rotor blade.

4. High-dimensional model representations of the response are found to approximate the computational aeroelastic model for uncertainty analysis. Monte Carlo simulations with the HDMR models and direct simulations produce similar results. Therefore, Monte Carlo simulations with a very large number of samples (one hundred thousand) are performed with HDMR models in few minutes which can take approximately 1000 CPU hours with the direct simulations. Further, it is found from the authors' previous studies that HDMR with $s = 5$ or 7 works well for most of the problems. Due to this fact, results for $s = 7$ are used in this paper to construct HDMR models and found to produce good meta-model approximations.
5. Spatially uncertain rotor blade properties have a considerable influence on the vibratory load predictions of the helicopter. Longitudinal and lateral vibratory forces show deviations up to 20 percent from their baseline value. The vertical vibratory force is highly sensitive to uncertainty with maximum deviations up to 60 percent from its baseline value. The rolling and pitching moments are less sensitive to uncertainty whereas the vibratory yawing moment shows a scattering of up to 60 percent. Further, the PDFs of vibratory loads show non-Gaussian type distributions.

Acknowledgements

The authors acknowledge the support of the European Research Council through project 247045 entitled "Optimisation of Multi-scale Structures with Applications to Morphing Aircraft."

References

[1] P.J. Attar, E.H. Dowell, Stochastic analysis of a nonlinear aeroelastic model using the response surface method, Journal of Aircraft 43 (4) (2006) 1044–1052.
[2] I. Babuška, P. Chatzipantelidis, On solving linear elliptic stochastic partial differential equations, Computer Methods in Applied Mechanics and Engineering 191 (37–38) (2002) 4093–4122.
[3] I. Babuska, K. Liu, R. Tempone, Solving stochastic partial differential equations based on the experimental data, Mathematical Models & Methods in Applied Sciences 13 (3) (2003) 415–444.
[4] G. Bir, I. Chopra, University of Maryland Advanced Rotorcraft Code (UMARC) theory manual, Tech. Rep. UM-AERO Report 92-02, 1992.
[5] F. Borello, E. Cestino, G. Frulla, Structural uncertainty effect on classical wing flutter characteristics, Journal of Aerospace Engineering 23 (4) (2010) 327–338.
[6] L. Bruno, C. Canuto, D. Fransos, Stochastic aerodynamics and aeroelasticity of a flat plate via generalised polynomial chaos, Journal of Fluids and Structures 25 (7) (2009) 1158–1176.
[7] R. Chowdhury, S. Adhikari, High dimensional model representation for stochastic finite element analysis, Applied Mathematical Modelling 34 (12) (2010) 3917–3932.
[8] R. Chowdhury, B.N. Rao, Assessment of high dimensional model representation techniques for reliability analysis, Probabilistic Engineering Mechanics 24 (1) (2009) 100–115.
[9] R. Chowdhury, B.N. Rao, A.M. Prasad, High dimensional model representation for piece-wise continuous function approximation, Communications in Numerical Methods in Engineering 24 (12, Sp. Iss. SI) (2008) 1587–1609.
[10] R. Chowdhury, B.N. Rao, A.M. Prasad, High-dimensional model representation for structural reliability analysis, Communications in Numerical Methods in Engineering 25 (4) (2009) 301–337.
[11] R. Ganguli, A survey of recent developments in rotorcraft design optimization, Journal of Aircraft 41 (3) (2004) 493–510.
[12] R. Ghanem, P. Spanos, Stochastic Finite Elements: A Spectral Approach, Springer-Verlag, New York, USA, 1991.
[13] M. Ghommem, M. Hajj, A. Nayfeh, Uncertainty analysis near bifurcation of an aeroelastic system, Journal of Sound and Vibration 329 (16) (2010) 3335–3347.
[14] W. Johnson, Helicopter Theory, Princeton University Press, New Jersy, 1980.
[15] G. Li, C. Rosenthal, H. Rabitz, High dimensional model representations, Journal of Physical Chemistry A 105 (33) (2001) 7765–7777.
[16] G. Li, S. Wang, H. Rabitz, S. Wang, P. Jaffe, Global uncertainty assessments by high dimensional model representations (HDMR), Chemical Engineering Science 57 (21) (2002) 4445–4460.
[17] N.J. Lindsley, P.S. Beran, C.L. Pettit, Effects of uncertainty on nonlinear plate aeroelastic response, AIAA Paper 2002-1271.
[18] S. Marques, K.J. Badcock, H. Haddad Khodaparast, J.E. Mottershead, Transonic aeroelastic stability predictions under the influence of structural variability, Journal of Aircraft 47 (4) (2010) 1229–1239.
[19] S. Murugan, R. Ganguli, D. Harursampath, Aeroelastic response of composite helicopter rotor with random material properties, Journal of Aircraft 45 (1) (2008) 306–322.
[20] S. Murugan, D. Harursampath, R. Ganguli, Material uncertainty propagation in helicopter nonlinear aeroelastic response and vibration analysis, AIAA Journal 46 (9) (2008) 2332–2344.
[21] A. Nouy, Generalized spectral decomposition method for solving stochastic finite element equations: Invariant subspace problem and dedicated algorithms, Computer Methods in Applied Mechanics and Engineering 197 (51–52) (2008) 4718–4736.
[22] A. Nouy, Recent developments in spectral stochastic methods for the numerical solution of stochastic partial differential equations, Archives of Computational Methods in Engineering 16 (3) (2009) 251–285.
[23] A.K. Onkar, C.S. Upadhyay, D. Yadav, Stochastic finite element buckling analysis of laminated plates with circular cutout under uniaxial compression, Journal of Applied Mechanics – Transactions of the ASME 74 (4) (2007) 798–809.
[24] P. Pawar, R. Ganguli, Genetic fuzzy system for damage detection in beams and helicopter rotor blades, Computer Methods in Applied Mechanics and Engineering 192 (16–18) (2003) 2031–2057.
[25] C.L. Pettit, Uncertainty quantification in aeroelasticity: Recent results and research challenges, Journal of Aircraft 41 (5) (2004) 1217–1229.
[26] F. Poirion, On some stochastic methods applied to aeroservoelasticity, Aerospace Science and Technology 4 (3) (2000) 201–214.
[27] H. Rabitz, O. Alis, General foundations of high-dimensional model representations, Journal of Mathematical Chemistry 25 (2–3) (1999) 197–233.
[28] B.N. Rao, R. Chowdhury, Enhanced high-dimensional model representation for reliability analysis, International Journal for Numerical Methods in Engineering 77 (5) (2009) 719–750.
[29] C. Siva, M.S. Murugan, R. Ganguli, Effect of uncertainty on helicopter performance predictions, Proceedings of the Institution of Mechanical Engineers, Part G, Journal of Aerospace Engineering 224 (5) (2010) 549–562.
[30] I. Sobol, Theorems and examples on high dimensional model representation, Reliability Engineering & System Safety 79 (2) (2003) 187–193.
[31] O. Soykasap, Inverse method in tilt-rotor optimization, Aerospace Science and Technology 5 (7) (2001) 437–444.
[32] S. Sriramula, M.K. Chryssanthopoulos, Quantification of uncertainty modelling in stochastic analysis of FRP composites, Composites Part A: Applied Science and Manufacturing 40 (11) (2009) 1673–1684.
[33] B. Sudret, A. Der-Kiureghian, Stochastic finite element methods and reliability, Tech. Rep. UCB/SEMM-2000/08, Department of Civil & Environmental Engineering, University of California, Berkeley, November 2000.
[34] E. Vanmarcke, Random Fields: Analysis and Synthesis, The MIT Press, Cambridge, MA, 1993.
[35] S.R. Viswamurthy, R. Ganguli, An optimization approach to vibration reduction in helicopter rotors with multiple active trailing edge flaps, Aerospace Science and Technology 8 (3) (2004) 185–194.
[36] C. Wu, H. Zhang, T. Fang, Flutter analysis of an airfoil with bounded random parameters in incompressible flow via Gegenbauer polynomial approximation, Aerospace Science and Technology 11 (7–8) (2007) 518–526.